

SPATIOTEMPORAL CHAOS IN ONE- AND TWO-DIMENSIONAL COUPLED MAP LATTICES

Kunihiko KANEKO*

Center for Complex Systems Research, University of Illinois at Urbana-Champaign, Champaign, IL 61820, USA and Center for Nonlinear Studies, Los Alamos National Laboratory, Los Alamos, NM 87545, USA

Coupled map lattices are investigated as a model for spatiotemporal chaos. Pattern dynamics in diffusively coupled logistic lattice is briefly reviewed with the use of power spectra, domain distribution, and Lyapunov spectra. Mechanism of pattern selection with the suppression of chaos is discussed. Pattern dynamics on a 2-dimensional lattice is shown. In a weak coupling regime, a similarity with the one-dimensional case is found; frozen random pattern, pattern selection, Brownian motion of a chaotic string, and intermittent collapse of the pattern with selective flicker noise. In a strong coupling regime, frozen pattern is found to be unstable by the surface tension, which is in contrast with the one-dimensional case. Convective coupling model is introduced in connection with the fluid turbulence of Navier–Stokes type. Soliton turbulence and vortex turbulence in the model are reported. Physical implications of coupled map lattices are discussed.

1. Introduction

Modelling and characterization of complex phenomena in space–time is important in the study of turbulence in a general sense, not only in fluid dynamics but also in solid-state physics, optics, chemical reaction with diffusion, and possibly in biology. This kind of phenomena is called as “spatiotemporal chaos”, in an attempt to understand it on the basis of knowledge on dynamical systems theory, especially, chaos.

The author has been investigating spatiotemporal chaos under the following strategy:

- (1) proposition of a simple and essential model for spatiotemporal chaos;
- (2) global search of qualitative pattern dynamics using various visualization techniques [4] and exploration of the universal scenario for pattern dynamics [1];
- (3) quantitative description of the change of pattern dynamics with the use of spatiotemporal

power spectra, domain distribution as order parameters, Lyapunov spectra and vectors, co-moving Lyapunov spectra, and so on [1];

(4) construction of a theory for spatiotemporal chaos based on the statistical mechanics for chaos and for a system with many degrees of freedom (e.g., spin systems), including an attempt towards a marriage between Perron–Frobenius operator and mean field theory;

(5) application to physical, chemical and biological systems: e.g., Bénard convection, convection in liquid crystals, Taylor vortex, open flow in fluid systems, chemical reaction with diffusion, some solid-state systems such as Josephson junction array, charge density wave, spin wave turbulence, spinodal decomposition, and possibly some biological networks.

Here we mainly focus on (2) and (3) and briefly refer to (4) and (5). The model we use here is a coupled map lattice (CML), which has been introduced in the reasons listed in [1–4], and has been investigated in various contexts recently [5–12].

A CML is a dynamical system with a discrete time, discrete space, and continuous state [1–5] (see also, [7–12]). A modelling of physical phe-

*On leave from: Institute of Physics, College of Arts and Sciences, University of Tokyo, Komaba, Meguro-ku, Tokyo 153, Japan.

nomena by CML is based on the following steps:

(A) Decompose the phenomena into independent units (e.g., convection, reaction, diffusion, and so on).

(B) Replace each unit by the possible simplest parallel dynamics on a lattice: the dynamics consists of a transformation on each lattice point or a coupling term among suitably chosen neighbors.

(C) Carry out each unit dynamics (“procedure”) successively.

The following diffusively coupled model has been frequently investigated:

$$x_{n+1}(i) = (1 - \epsilon)f(x_n(i)) + \epsilon/2[f(x_n(i+1)) + f(x_n(i-1))], \quad (1)$$

where n is a discrete time step and i is a lattice point ($i = 1, 2, \dots, N = \text{system size}$) with a periodic boundary condition. Extensions to a higher-dimensional lattice and to a model of a different type of coupling (“convective coupling”) will be studied in sections 4 and 5. Here the mapping function $f(x)$ is chosen to be the logistic map:

$$f(x) = 1 - ax^2. \quad (2)$$

In this model, the independent procedures in (B) are local transformation (eq. (2)) and the diffusion process (eq. (1)), which are separated parallel procedures. The model consists of the sequential repetition of these two procedures. This argument leads to the following equivalent form with the above model:

$$x_{n+1}(i) = f((1 - \epsilon)x_n(i) + \epsilon/2(x_n(i+1) + x_n(i-1))). \quad (3)$$

The separation of procedure makes it possible to obtain inverse images of the dynamics. The preimages of our dynamics is constructed as follows: Note that the inverse process is just the combination of (1) the inverse of spatial average and (2) the inverse images of local dynamics. The first process is just a calculation of the inverse of

the tridiagonal matrix for diffusive coupling:

$$x'(j) = \sum_l (1/N) \sum_k \frac{\exp(2ik\pi(l-j)/N)}{1 - 2\epsilon \sin^2 k\pi/N} x(l) \equiv \sum_l a_{jl} x(l). \quad (4)$$

The second process is just $x''(j) = f^{-1}(x'(j))$, where $f^{-1}(x)$ is inverse function of $f(x)$, (for the logistic map (2) it is given by $\pm \sqrt{(1-x)/a}$). Thus the preimages are given by $x_{n-1}(j) = f^{-1}(\sum_l a_{jl} x_n(l))$. This simple procedure for the preimages is essential in the construction of statistical mechanics by Perron–Frobenius operator.

Another important feature in this model is as follows: if a state x_j^* is a stable periodic cycle for a single map $x' = f(x)$, then the homogeneous solution $x(i) = x_j^*$ is also stable, for “physical” ϵ values, i.e., $\epsilon < 2/3$. If we took other coupling forms, this stability of a homogeneous periodic state would not be guaranteed.

A perturbation theory to derive a CML from a coupled ordinary differential equation was carried out by Yamada and Fujisaka [7], which leads to a model (1) within a certain condition. Another derivation of CML from a partial differential equation is the use of interaction term $F(x(r)) \times \sum_n \delta(t-n)$, as is frequently used in the derivation of standard mapping from a Hamiltonian system [13].

A construction of a toy model for fluid dynamics using this separation of procedures is introduced in section 5 where successive procedures are convection, diffusion, and damping.

2. Brief review on pattern dynamics

Here we briefly review phases of the one-dimensional logistic lattice (1). For detailed accounts see [1]. The essential change of a spatiotemporal pattern in our model with the increase of nonlinearity is (i) frozen random state, (ii) pattern selection and (iii) fully developed spatiotemporal chaos (see fig. 1 of [1] for the phase diagram). Change of each

Table I
Characterization of phases by the quantifiers. See text for the detail.

Phase \ Quantifiers	Temporal power spectra	Spatial power spectra	Pattern distribution $Q(k)$	Pattern entropy S_p	Dynamical entropy S_d	Lyapunov spectra	KS entropy
Frozen random pattern	peaks + broad band noise (fig. 1(a))	$\exp(-\text{const.} \times k)$ (fig. 2(a))	$Q(k) \neq 0$ for many k 's (fig. 3(a))	large (almost constant)	0	small stepwise structure	positive
Pattern selection	peaks + broad band noise (fig. 1(b, c))	few peaks (+ noise) (fig. 2(b))	few $Q(k)$'s $\neq 0$ ($Q(l) = 0$ for $l > l_c$) (fig. 3(b))	small (decreasing)	0	large stepwise structure	small (decreasing) (or 0)
Fully developed turbulence	broad band noise (fig. 1(d))	$\exp(-\text{const.} \times k^2)$ (fig. 2(d))	$Q(k) \propto \exp(-\text{const.} \times k)$ (fig. 3(c))	large (increasing)	large $S_d \approx S_p$	smooth function	large (increasing)

state is characterized by power spectra, distribution of domains, entropy, and Lyapunov spectra. Results are summarized in table I and figs. 1–3.

Here temporal power spectra are the power of Fourier transform of a time series of $x(i)$:

$$P(\omega) = \left\langle \left\langle \left| \sum_{n=t_0}^{t_1} x_n(j) e^{2\pi i n \omega} \right|^2 \right\rangle \right\rangle; \quad (5)$$

For a frozen random pattern, the peak at $\omega = 1/2$ is seen as is expected (fig. 1a), since a single logistic map exhibits a period-2 band motion for this parameter range. In the pattern selection regime, still the peak (and some other peaks for some parameters) is observed (fig. 1(b, c)), which is due to the regular motion by the pattern selection mechanism. (Note that in this parameter value of a , a single logistic map cannot show the motion of period-2 band.) In the fully developed regime, the peak no more exists and is replaced by some Lorentzian band noise around it and around $\omega \approx 0$ (fig. 1(d)).

Spatial power spectra are obtained by spatial Fourier transform of a pattern:

$$S(k) = \left\langle \left\langle \left| (1/N) \sum_{j=1}^{j=N} x_n(j) e^{2\pi i k j / N} \right|^2 \right\rangle \right\rangle. \quad (6)$$

In the frozen random phase, they show roughly $\exp(-\text{const.} \times k)$ (fig. 2(a)), which is due to the domain distribution with a long tail. In the selection regime, a diffuse peak at $k = k_p$ appears, corresponding to the inverse of the selected domain size (fig. 2(b)). As the nonlinearity is increased the broad band around $k \approx 0$ develops (fig. 2(c)), till they show the form given by random generation of domains (fig. 2(d)) in the fully developed regime.

Domain size is defined as the length of spatial sequence in which $(x_n(i) - x^*)$ has the same sign [1], where x^* is an unstable fixed point of the logistic map, which separates the two-band motion: $x^* = (\sqrt{1 + 4a} - 1)/(2a)$. The distribution function $Q(k)$ of domains is a probability distribution of the domain size sampled over the total lattice. For a frozen random pattern, there are a lot of possible domain sizes (fig. 3(a); maximum domain size (43 in the figure) increases with the increase of total lattice size), while only few domain sizes are possible in the pattern selection regime (fig. 3(b); note that for domain sizes larger than 12, the distribution vanishes, which is invariant with the change of system size). In the fully developed regime, $Q(k)$ behaves as $\exp(-\text{const.} \times k)$, which clearly illustrates the random generation of domains (fig. 3(c)).

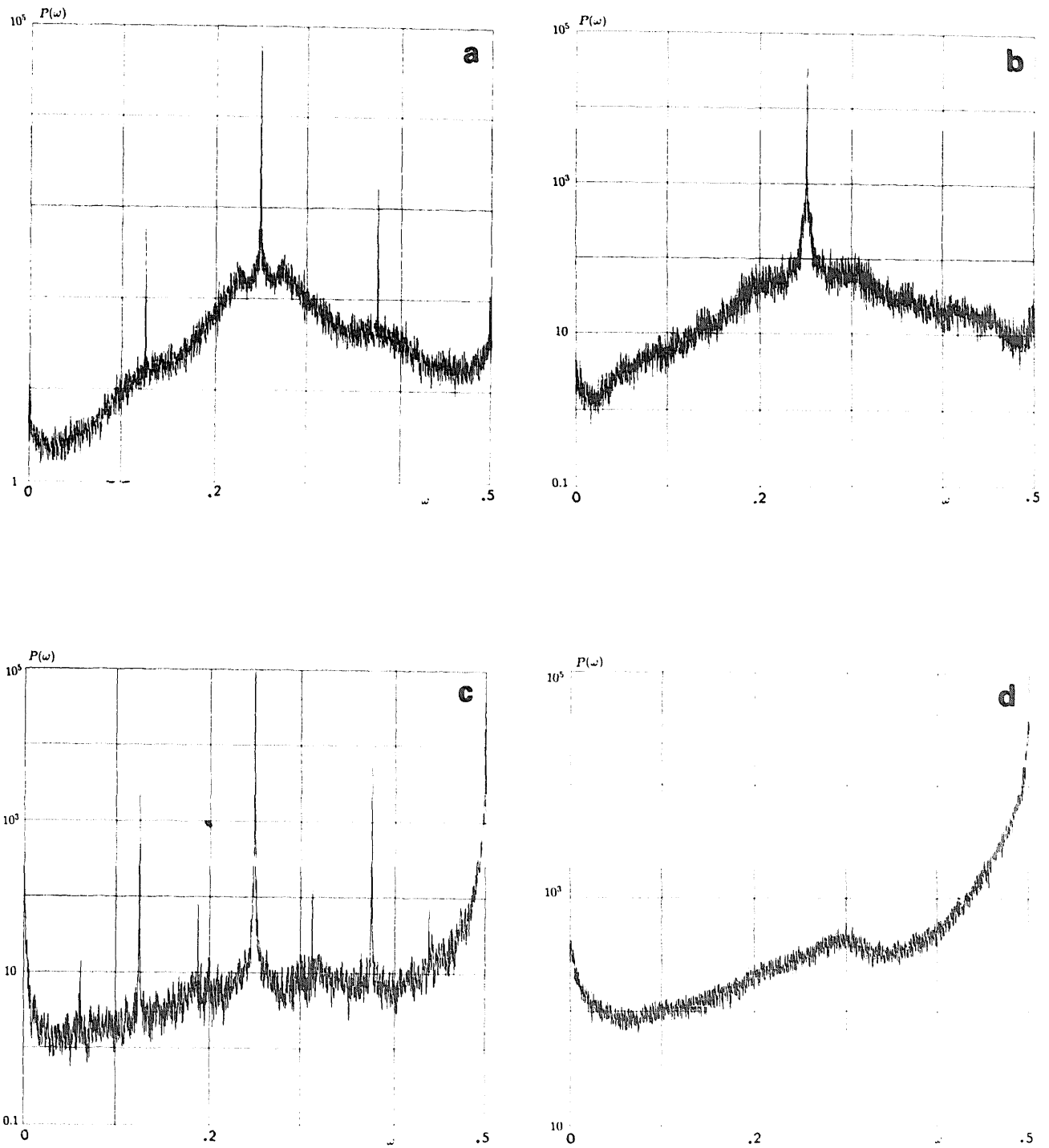


Fig. 1. Semilog plot of temporal power spectra $P(\omega)$ for the model (1.1), with $\epsilon = 0.3$, $N = 256$, and starting with a random initial condition. Calculated from 4096 time step averages after discarding 10000 transients. Averaged from 64 lattice points. (a) $a = 1.53$; (b) $a = 1.58$; (c) $a = 1.7$; (d) $a = 1.83$.

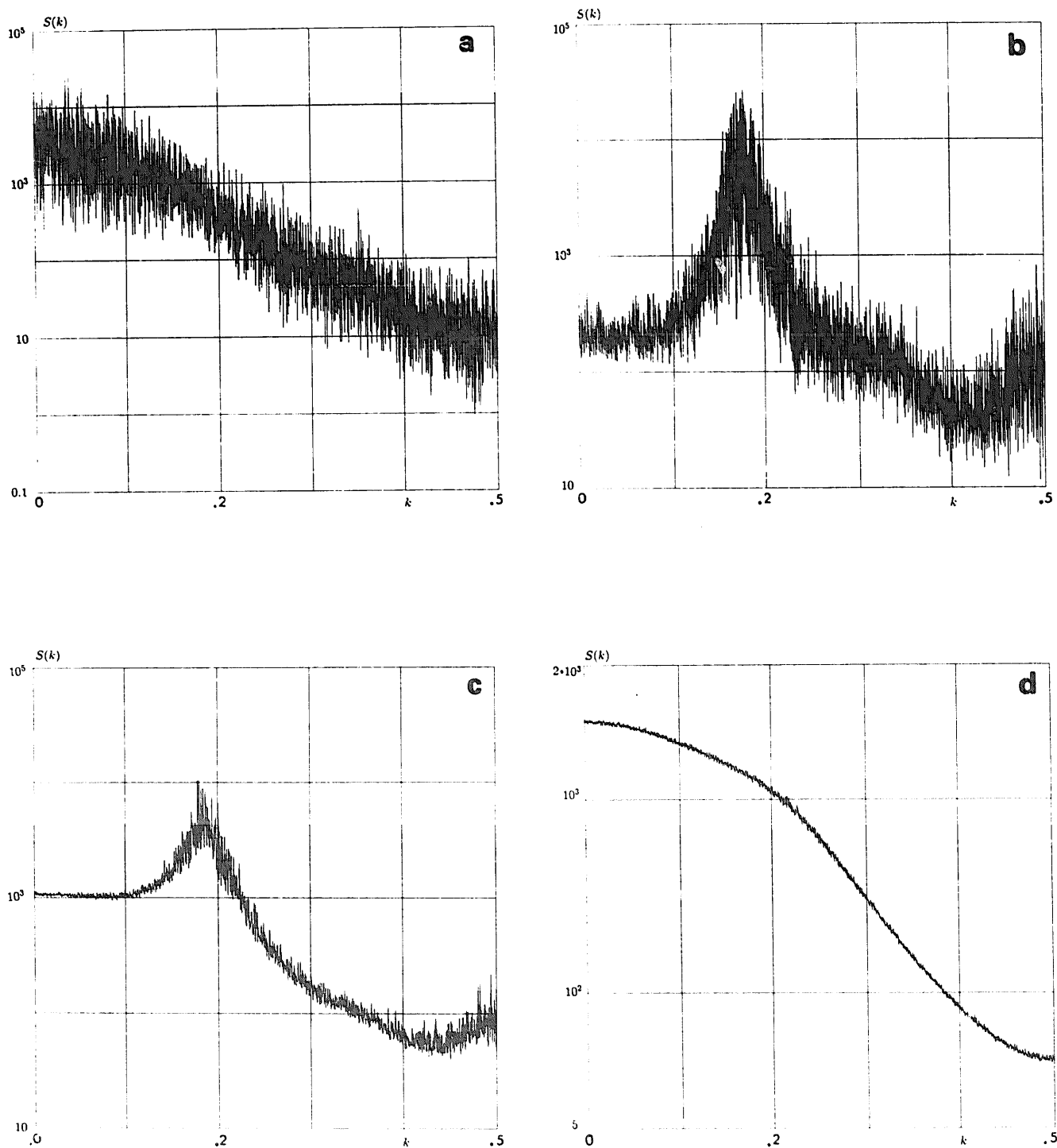


Fig. 2. Semilog plot of spatial power spectra $S(k)$ for the model (1.1), with $\epsilon = 0.3$, $N = 4096$, and starting with a random initial condition. Calculated from 10000 time step averages after discarding 10000 transients. (a) $a = 1.53$; (b) $a = 1.69$; (c) $a = 1.74$; (d) $a = 1.94$.

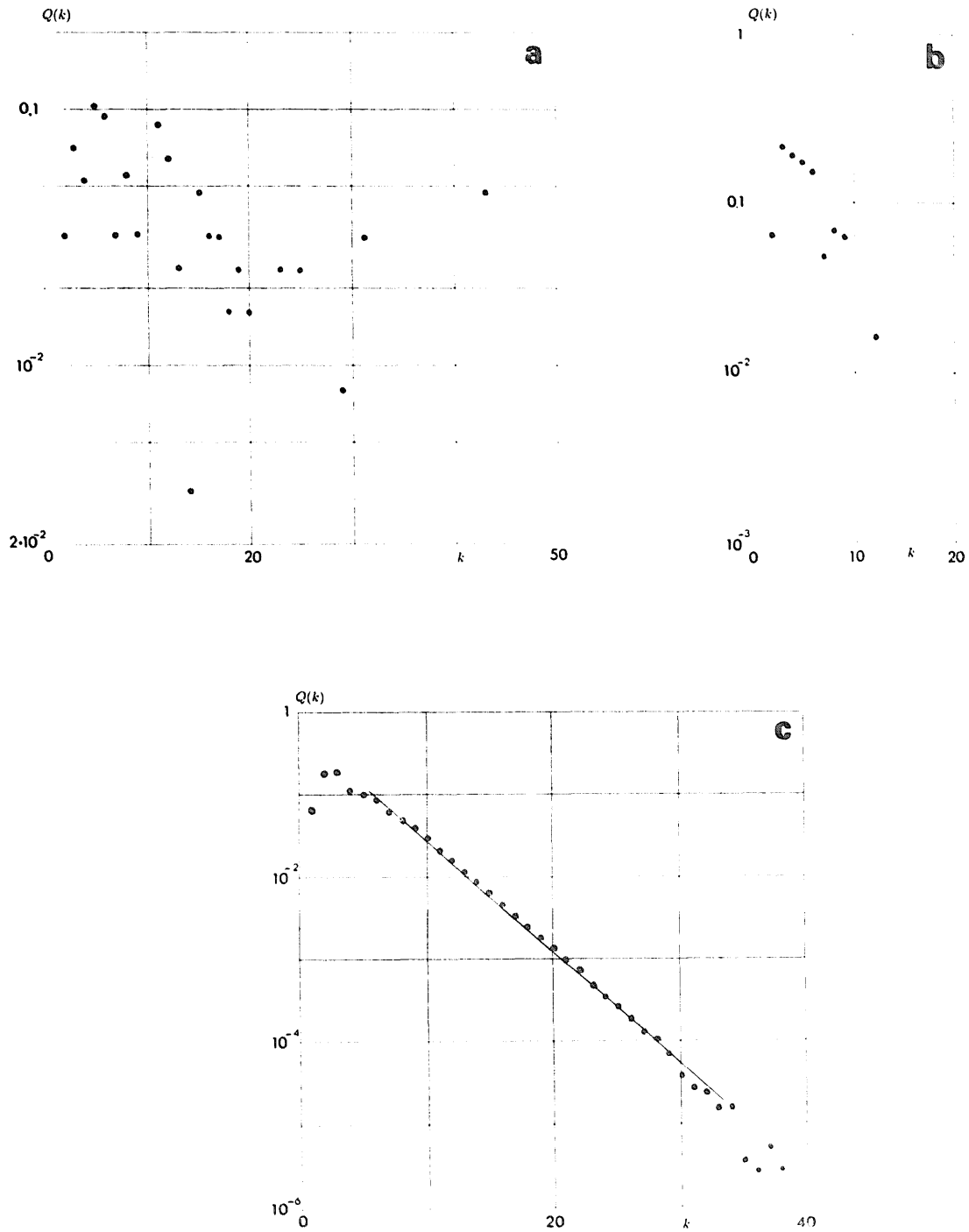


Fig. 3. Semilog plot of pattern distribution function $Q(k)$ for the model (1.1) with $\epsilon = 0.3$, $N = 1000$ and starting with random initial conditions. $Q(k)$ is calculated from the average for 8000 steps sampled per 8 time steps, after 10,000 transients. (a) $a = 1.549$; ($N = 1000$); (b) $a = 1.57$ ($N = 1000$); (c) $a = 1.88$ ($N = 4096$).

As usual, pattern entropy is defined by $-\sum Q(k) \log(Q(k))$, which characterizes a variety of possible static patterns. The dynamical entropy is defined by the mutual information between two successive patterns with a given time interval (see [1]).

In a frozen random phase, pattern entropy is rather large, and takes almost a constant value. As the nonlinearity is increased, it shows a remarkable decrease at the pattern selection, and again increases in the fully developed regime. A dynamical entropy vanishes at the frozen random and pattern selection regimes. It increases in the fully developed regime.

Lyapunov spectra are calculated from the eigenvalues of products of Jacobi matrices [6]. From the sum of positive exponents, Kolmogorov–Sinai (KS) entropy is estimated. In our lattice system the density of KS entropy is a more relevant quantifier, which is calculated by the division by the system size N . A salient feature in the pattern selection regime is the decrease of KS entropy with the increase of nonlinearity.

Interesting phenomena occur at the transition from (i) to (ii) and from (ii) to (iii) [1]. The former is treated in the next section, while the latter is known to belong to a class of phenomena called “spatiotemporal intermittency” (for spatiotemporal intermittency see [2, 4, 15, 16, 17, 11, 1]). Here we note that an experiment of a Bénard convection in an annulus shows a similar behavior with a pattern competition intermittency in our model, in its spatiotemporal pattern, power-law distribution of the cluster at the onset, and temporal/spatial power spectra [20]. This may not be surprising, since our model is one of the simplest which has local chaotic motion and diffusion. A possible relation of spatiotemporal intermittency with transient turbulence [21] is discussed in [22].

3. Pattern selection: glass–crystal transition?

Here we study the mechanism of pattern selection in a little more detail.

The phenomena which occur at the pattern selection regime are summarized as follows:

(1) decrease of possible domain sizes: for $a < a_p \approx 1.54$, domains of larger sizes appear as the system size is increased. For $a > a_p$, there exists an upper bound of domain size $l_c(a)$ independent of a system size, such that domains larger than $l_c(a)$ cannot exist. $l_c(a)$ depends on a and decreases with the increase of a . See fig. 3(b,c) for examples of domain distribution. Decrease of the variety of domain size is clearly seen in the decrease of static pattern entropy. Onset of decrease at $a = a_p$ is clearly seen in fig. 4.

(2) Suppression of chaos by pattern selection: this is seen in the decrease of KS entropy at $a > a_p$ [1]. This suggests that the chaos is suppressed by the pattern selection process. A way of viewing the temporal process of the decrease of chaos is the use of local space–time Lyapunov exponents, introduced by Umberger and the author [23]. Local space–time Lyapunov exponents are calculated by the products of Jacobi matrices for a given subsystem (size $2L + 1$) over finite

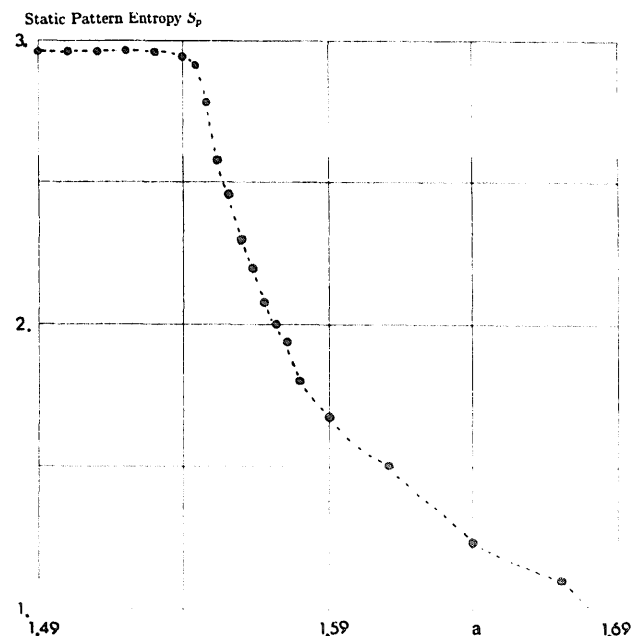


Fig. 4. Pattern (static) entropy as a function of a , near the pattern selection transition: Note the onset of decrease of entropy at $a = a_p$, $\epsilon = 0.3$, $N = 10000$ and starting with random initial conditions. Calculated from $Q(k)$ obtained through 1000 steps sampled per 8 time steps, after 10000 transients.

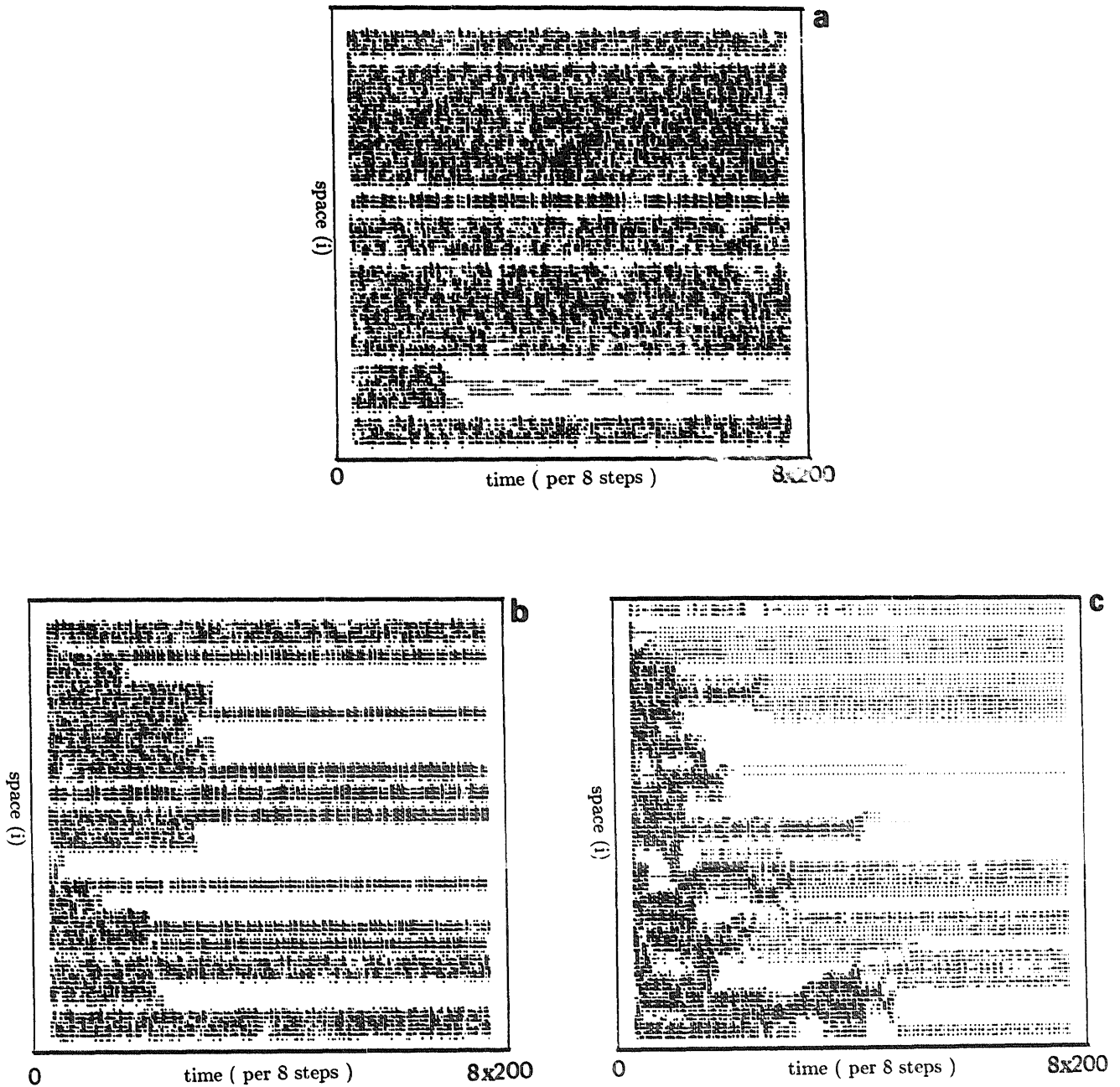


Fig. 5. Spatiotemporal Lyapunov exponent diagram: Local space-time Lyapunov exponent for each lattice point and time is shown. In each space-time pixel, a box is plotted whose length is proportional to the corresponding local Lyapunov exponent only if it is positive, otherwise the pixel is left blank. Lattice size = 100. For time steps 0 to 200×8 . Local Lyapunov exponent is calculated by a subspace size 3 ($L = 1$) and time steps 8. (a) $a = 1.54$, $\epsilon = 0.3$; here maximum of the exponent in the figure is 0.400 and the minimum is -0.686 . (b) $a = 1.58$, $\epsilon = 0.3$; here maximum of the exponent in the figure is 0.474 and the minimum is -1.126 . (c) $a = 1.70$, $\epsilon = 0.3$; here maximum of the exponent in the figure is 0.534 and the minimum is -1.208 .

4. Pattern dynamics in a 2-dimensional lattice

Extension of our CML with diffusive coupling to a two-dimensional lattice in space is quite straightforward. Here we consider the simplest case, i.e., nearest-neighbor coupling on a square

lattice (see also [24]). The model is given by

$$\begin{aligned} x_{n+1}(i, j) &= (1 - \epsilon)f(x_n(i, j)) \\ &+ \epsilon/4[f(x_n(i+1, j)) + f(x_n(i-1, j)) \\ &+ f(x_n(i, j+1)) + f(x_n(i, j-1))], \end{aligned} \quad (8)$$

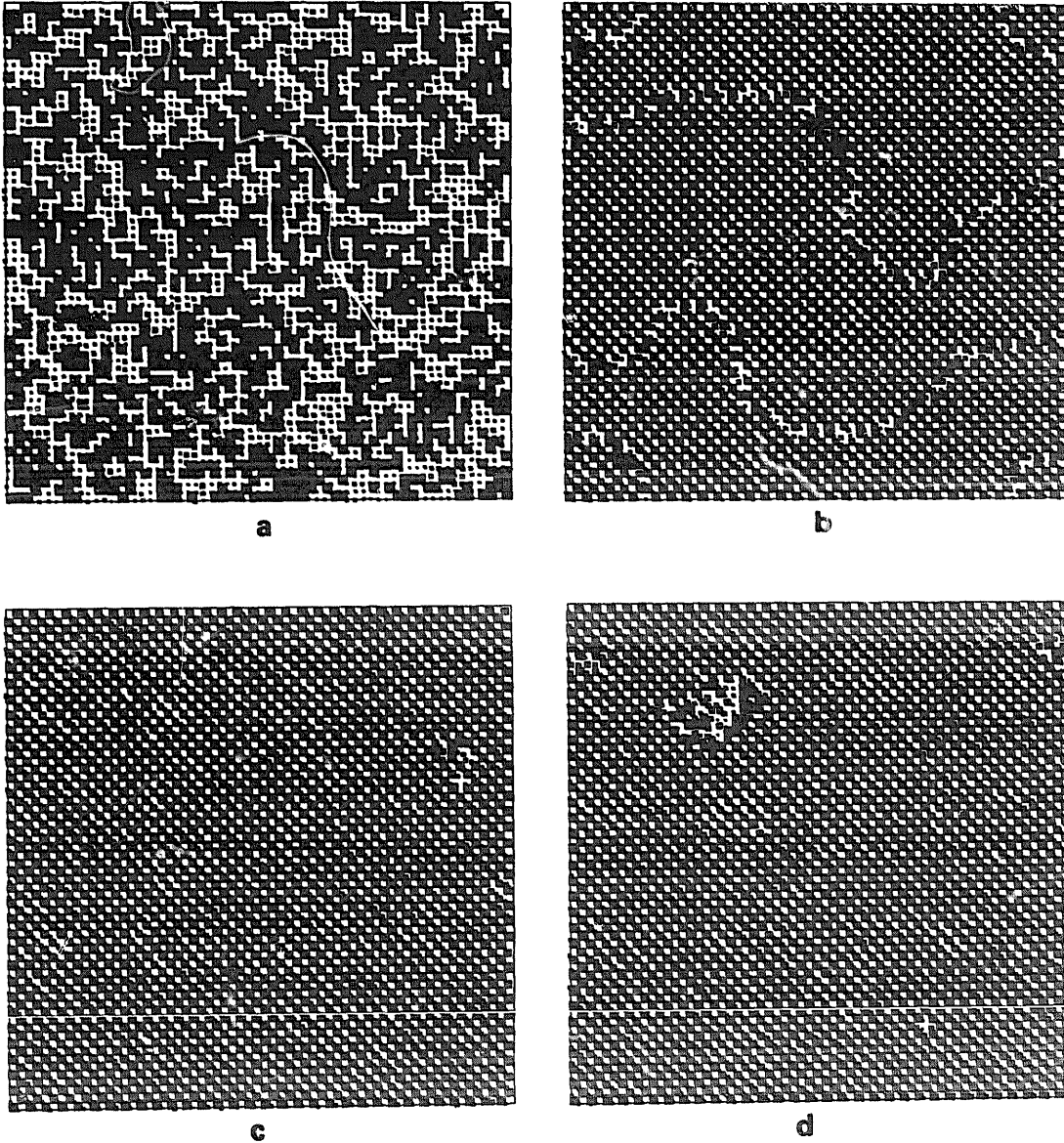


Fig. 6. Snapshot pattern for 2-dimensional lattice on a lattice point (i, j) a square with a length proportional to $(x_n(i, j) - 0.2)$ is depicted if $x_n(i, j) > 0.2$. Otherwise it is left blank. (a) $a = 1.5$, $\epsilon = 0.1$, size = 64×64 , at time step 1000; (b) $a = 1.85$, $\epsilon = 0.1$, size = 64×64 , at time step 2000. (c) $a = 1.901$, $\epsilon = 0.1$, size = 64×64 , at time step 91 500; (d) $a = 1.901$, $\epsilon = 0.1$, size = 64×64 , at time step 92 200; (e) $a = 1.903$, $\epsilon = 0.1$, size = 64×64 , at time step 100 000; (f) $a = 1.6$, $\epsilon = 0.2$, size = 32×32 , at time step 1200; (g) $a = 1.95$, $\epsilon = 0.2$, size = 32×32 , at time step 570 000; (h) $a = 1.94$, $\epsilon = 0.18$, size = 64×64 , at time step 8000; (i) $a = 1.93$, $\epsilon = 0.15$, size = 64×64 , at time step 18 000; (j) $a = 1.6$, $\epsilon = 0.5$, size = 32×32 , at time step 5000.

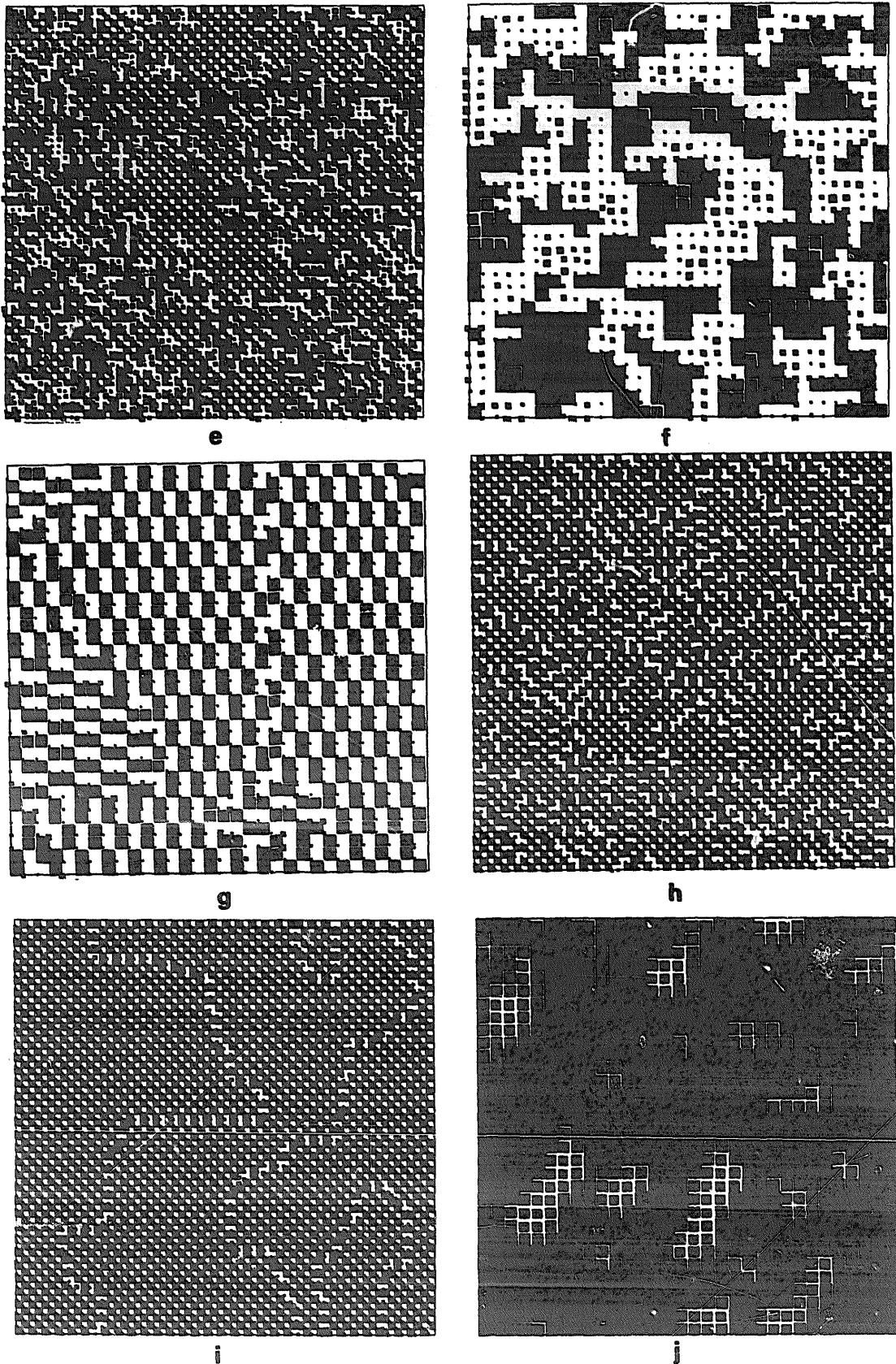


Fig. 6. Continued.

where n is a discrete time step and i, j denotes a 2-dimension lattice point ($i, j = 1, 2, \dots, N =$ system size) with a periodic boundary condition. Here the mapping function $f(x)$ is again chosen to be the logistic map $f(x) = 1 - ax^2$.

Examples of snapshots are shown in fig. 6.

For small ϵ , we have again observed the transition sequence from (i) frozen random state to (ii) pattern selection and to (iii) fully developed spatiotemporal chaos via spatiotemporal intermittency.

4.1. Checkerboard pattern selection, chaotic string, and intermittent collapse

For $\epsilon = 0.1$, a frozen random pattern is observed for $a < 1.75$ (fig. 6(a)). Checkerboard pattern is selected for $1.75 \leq a \leq 1.9$ (note that this range of parameters for the pattern selection agrees with the range for pattern selection in a 1-d lattice for the same value of coupling ϵ). See fig. 6(b) for an example. After some iterations (10^4 for a lattice 64×64), a single checkerboard pattern covers the whole lattice if the size is even. The selection process is regarded as the pattern formation, since two antiphased checkerboard domains are separated by a string, which moves chaotically in time and moves around space, and disappears by collisions.

In fig. 7, only the regions are depicted which do not belong to a checkerboard pattern. We can see the pattern formation process by the Brownian motion of chaotic string. Here we call the motion as Brownian, since the motion there obeys the normal diffusive behavior triggered by random walk [18]. The reason why we call it chaotic string is that the motion in a string shows a deterministic chaotic motion in the sense of positive Lyapunov exponent, as can be seen in the calculation of the following Lyapunov exponent.

The chaos of a string is quantitatively measured by taking a system of odd size (e.g., 7×7), where a single chaotic string which separates two anti-

phased checkerboards always exists. In fig. 8(a) the maximum Lyapunov exponent and KS entropy density for 8×8 lattice and 7×7 lattices are shown. The discrepancy between the two is seen for $1.75 \leq a \leq 1.9$, where a checkerboard pattern stably exists. Positive exponents for 7×7 lattice show the chaotic motion of a string clearly.

At $a = a_c = 1.901$, the checkerboard pattern collapses spontaneously. Defects are created spontaneously from a checkerboard pattern. For $a \approx 1.901$, these defects are not percolated. As a is increased further, they propagate and interact with other defects (percolate [19]) and form the spatiotemporal intermittency. The spatiotemporal pattern there is understood as the intermittent transition between checkerboards and random patterns (see fig. 6(e) for a snapshot).

Still, the lifetime of checkerboard pattern is very long if a is close to a_c . Following the results in the one-dimensional case [11, 1], we calculated the dynamical form factor $P(k_x, k_y, \omega)$, power of the Fourier transform in space and time. As in the 1-d case, it shows the selective flicker noise [11, 1] for the wavenumber of a checkerboard pattern, i.e.,

$$P(k_x = 1/2, k_y = 1/2, \omega) = \omega^{-\alpha} \quad (9)$$

($\alpha \approx 1.9$) while neither the spectrum $P(k_x = 1/2, k_y \approx 0, \omega)$ nor $P(k_x \approx 0, k_y \approx 0, \omega)$ does show the divergence of low-frequency parts (see fig. 9(a, b, c)).

To sum up, the pattern dynamics for $\epsilon = 0.1$ is essentially understood as the extension of pattern dynamics in the 1-dimensional logistic lattice as for the transition sequence, zigzag (checkerboard) pattern selection, Brownian motion of defects (strings), and its intermittent collapse of the selected pattern.

Recently Nasuno et al. [25] have performed a beautiful experiment on the collapse of a grid pattern in the electric convection of liquid crystal. They have found the intermittent collapse of the grid pattern and the selective flicker noise for the

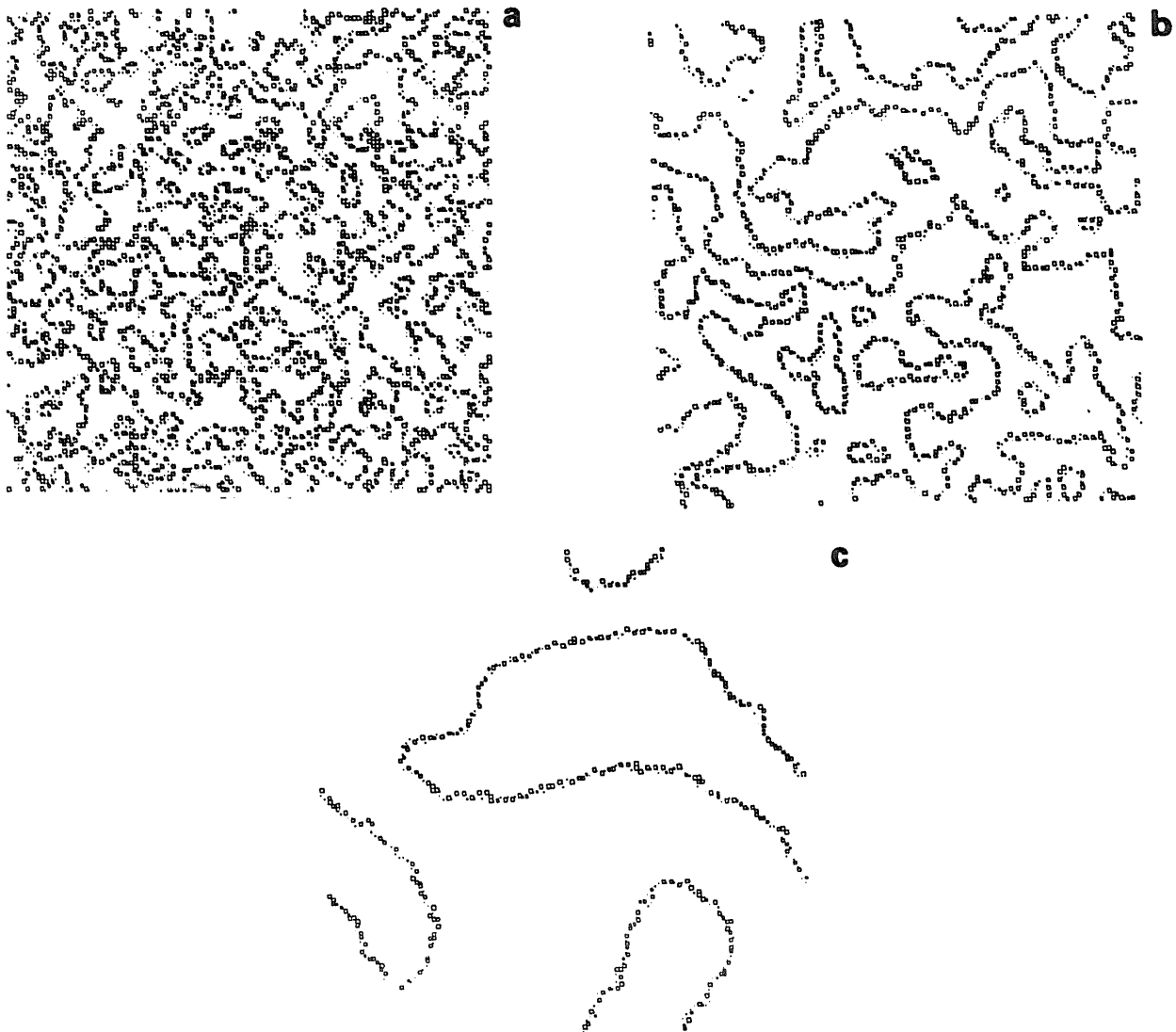


Fig. 7. Brownian motion of chaotic string: Only a lattice point which does not belong to a checkerboard pattern is depicted. Lattice size = 128×128 : $a = 1.8$, $\epsilon = 0.1$. (a) Time step = 96; (b) 416; (c) 18912.

wavenumber for the grid pattern (with $\alpha = 1.9$). Our observations in 1-d and 2-d logistic lattices show a good similarity with their results.

4.2. 2×1 pattern selection

For $\epsilon = 0.2$, we have again seen the frozen random pattern (fig. 6(f)), pattern selection, and fully developed spatiotemporal chaos. Here the selected pattern is a 2×1 unit (see fig. 6(g)). In the selection of 2×1 unit, the transient time necessary for

the pattern formation is much longer than that for a checkerboard pattern. Indeed, in fig. 6(f), after 570 000 steps, still a single domain has not yet covered the whole lattice, and a domain boundary is slowly moving. This slow pattern formation process is due to the 4-fold degeneracy of attractor (two types of phase of oscillation, and horizontal or perpendicular roll structure). The formation process is a competition among the 4 types of domains. This kind of pattern was first noted in a phase transition in 2-dimensional stochastic cellular automata [30].

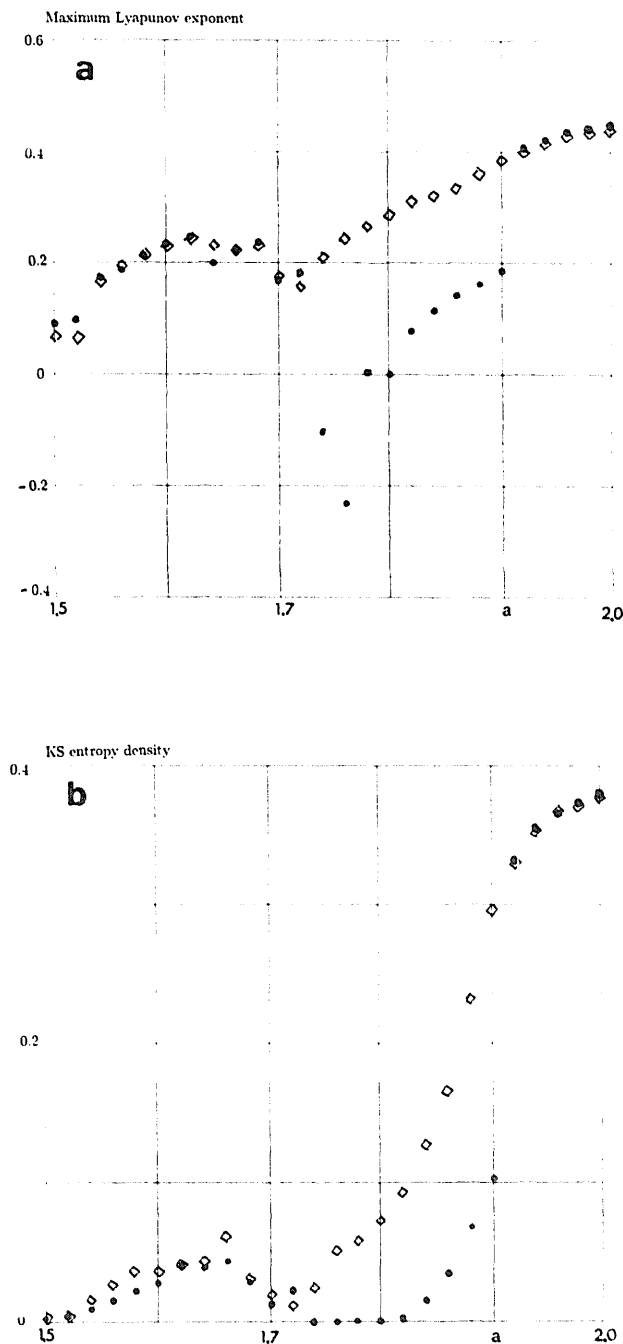


Fig. 8. KS entropy density (a) and maximal Lyapunov exponent (b) as a function of a for 2-dimensional logistic lattice of the size 7×7 (\diamond) and 8×8 (\ominus) with $\epsilon = 0.1$. Note the discrepancy for $1.74 \leq a \leq 1.90$, where a checkerboard pattern is selected. For the lattice of 7×7 , there is a chaotic string which separates the two neighboring domains out of phase, which gives additional positive Lyapunov exponents. Note that the motion of checkerboard is periodic or quasiperiodic for $1.74 \leq a \leq 1.81$. In the following figures Lyapunov exponents are calculated through the products of Jacobi matrices of the time step 2000 to 2500, starting from the random initial conditions.

Here again, chaos is suppressed by the pattern selection process. See fig. 10 for the change of maximum Lyapunov exponent and KS entropy density. Suppression of chaos is seen in the KS entropy density more clearly than in the maximum Lyapunov exponent. This is because the pattern selection is not complete. In fact, the motion of a boundary between two different 2×1 domains gives some positive Lyapunov exponents, which masks the decrease of maximal Lyapunov exponent. The number of positive exponents, on the other hand, is reduced drastically by the pattern selection, since the motion within a cluster of 2×1 with the same phase and direction is quasiperiodic (or with a slight chaotic modulation). Thus the KS entropy density is reduced by the selection.

As the nonlinearity is increased, collapse of the pattern by spatiotemporal intermittency again occurs. Here we note that the existence of 4-fold degeneracy strongly suggests the first order transition, which is true in a 2-dimensional stochastic cellular automaton [30].

In the coupling between 0.1 and 0.2 (e.g., 0.15), the competition between the checkerboard and 2×1 is seen, which leads to the intermittent collapse of the two patterns (pattern competition intermittency) (fig. 6(h)) or to the formation of chaotic string with 2×1 structure in the checkerboard cluster (fig. 6(i)). These are again similar to the observation in a 1-d lattice.

We note that the experiment by Nasuno et al., mentioned in the last subsection, also shows the competition of checkerboard ("grid") and 2×1 structure [25].

4.3. Absence of a frozen pattern for stronger coupling

For larger couplings such as $\epsilon > 0.3$, we have observed neither a frozen random pattern nor a pattern selection. A domain is unstable and a domain boundary moves in time till a single domain covers the whole lattice (fig. 6(j)).

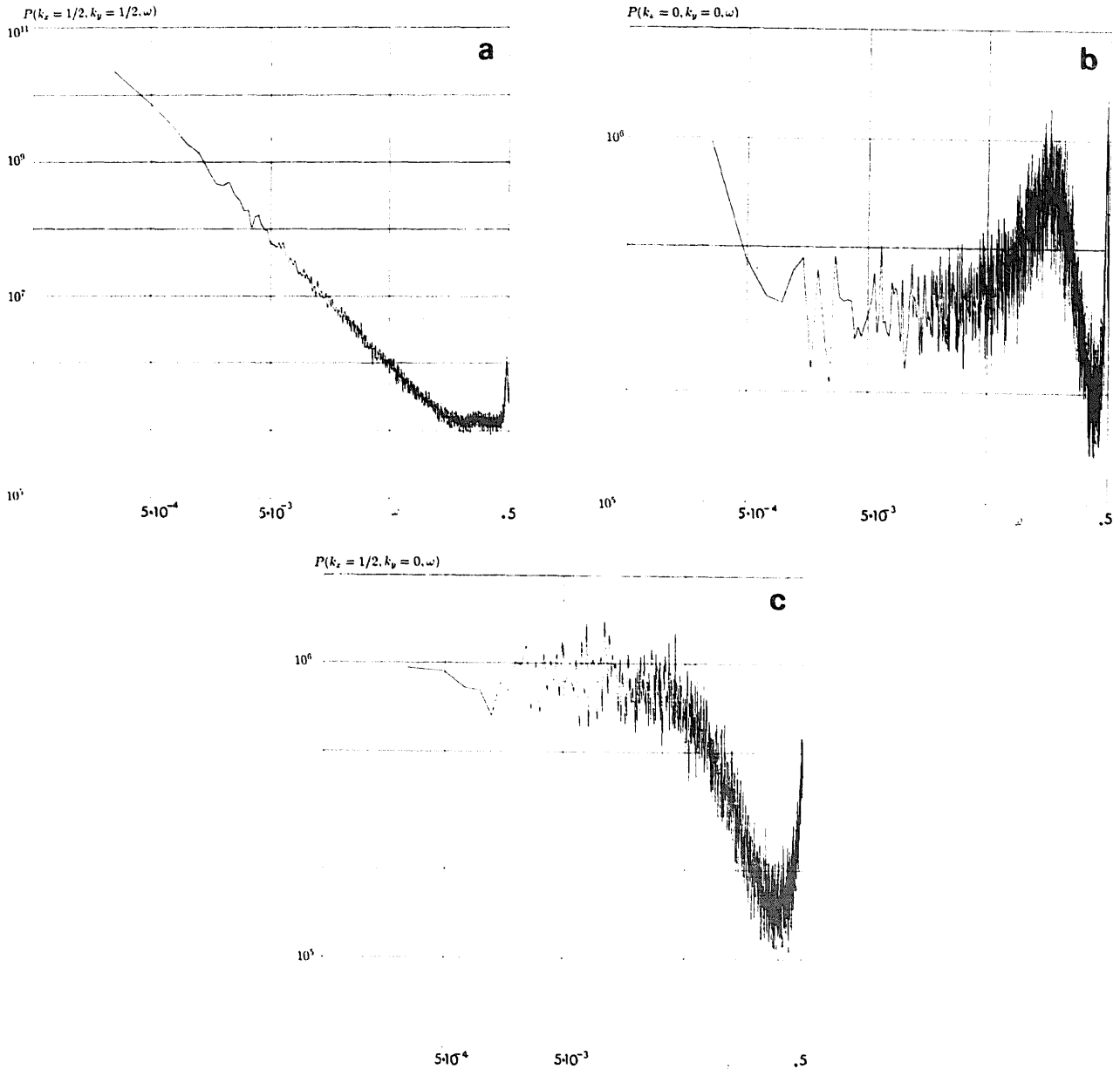


Fig. 9. Log-log plot of $P(k_x, k_y, \omega)$ as a function of ω . $a = 1.903$, $\epsilon = 0.1$. The spectrum is calculated for 50 sequential samples of 4096 steps after 2000 transients to a lattice of 32×32 . (a) $k_x = k_y = \frac{1}{2}$; (b) $k_x = k_y = 0$; (c) $k_x = \frac{1}{2}$, $k_y = 0$.

Change of Lyapunov exponents with the parameter a is smooth (fig. 11). Lyapunov spectra have a smooth shape for all a (fig. 12). From all of these results we can conclude that there are no pattern changes for strong coupling regimes in a 2-dimensional lattice (see also [27]).

The reason for the absence of frozen pattern is thought to be as follows: By the diffusive coupling, the domain boundary between two frozen

patterns has a tendency of diffusive motion. On the other hand, the motion in a domain is more stable than the boundary (recall that $x(i, j)$ at a domain boundary takes a value around the unstable fixed point of a logistic map), which leads to the tendency towards the preservation of a domain and the pinning of a boundary. The ratio of the former tendency to the latter increases with ϵ and with the dimension of a lattice. Here the

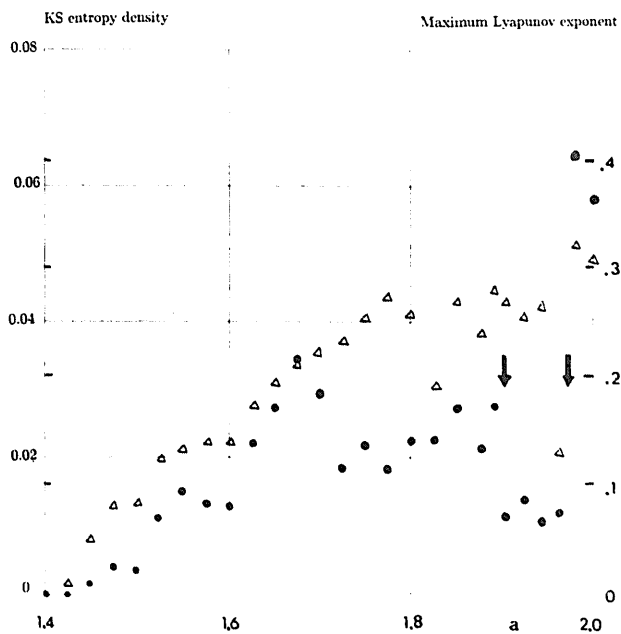


Fig. 10. KS entropy density (●) and maximal Lyapunov exponent (Δ) as a function of a for 2-dimensional logistic lattice of the size 10×10 with $\epsilon = 0.2$. In the parameter region between the arrows, pattern selection of 2×1 occurs.

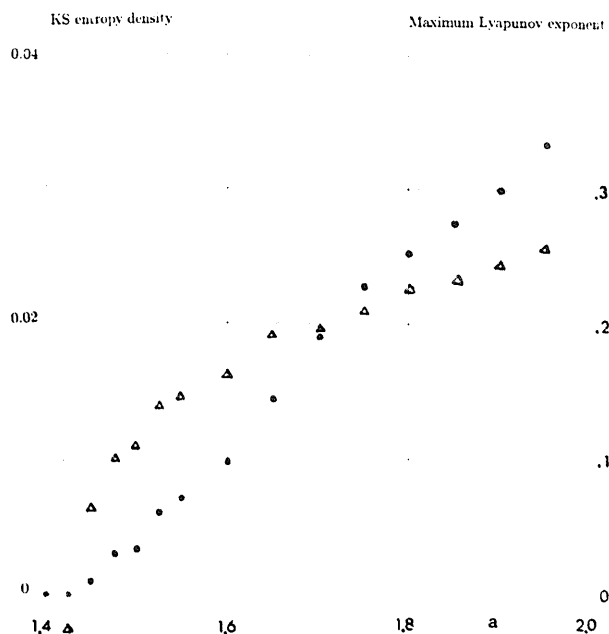


Fig. 12. KS entropy density (●) and maximal Lyapunov exponent (Δ) as a function of a for 2-dimensional logistic lattice of the size 10×10 with $\epsilon = 0.4$. Note the smooth increase with a , which is different from the results for $\epsilon = 0.1$ and $\epsilon = 0.2$.

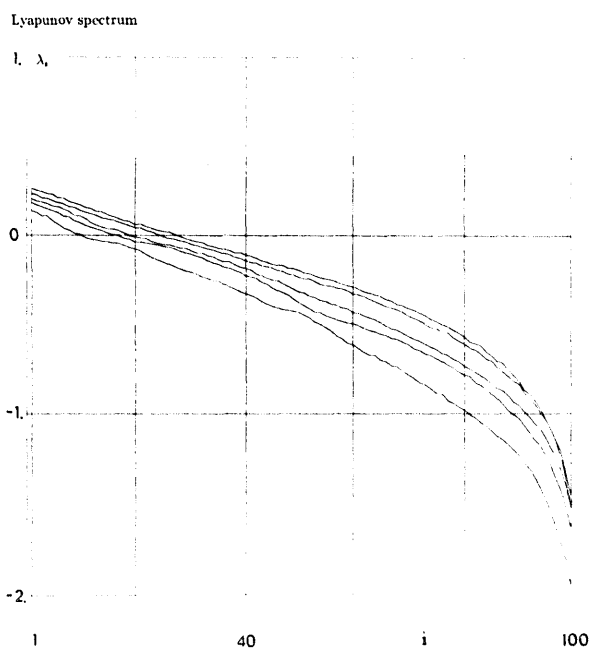


Fig. 11. Lyapunov spectra for the 2-dimensional logistic lattice of the size 10×10 with $\epsilon = 0.4$, $a = 1.55, 1.65, 1.75, 1.85,$ and 1.95 from the bottom to top.

estimate of the former boundary effect can be carried out as in the usual estimate of surface tension, which leads to $M^{(1-1/d)}$ for a domain of size M , for a d -dimensional lattice. For $d > 1$, a smaller domain has a smaller stability. Thus for a lattice with a dimension ≥ 2 , it is expected that a frozen random pattern or frozen pattern selection is unstable, for a stronger coupling. From our numerical results, it can be concluded that this threshold coupling lies around $\epsilon \approx 0.35$ for our 2-dimensional lattice with a nearest-neighbor coupling.

This feature (instability of frozen random pattern and nonexistence of frozen pattern selection) distinguishes the behavior in a 2-d lattice from that in 1-d.

5. Designing fluid dynamics with CML?

One difference between Navier–Stokes-type equation and our diffusively coupled map lattice

lies in that the nonlinearity in the former arises from the coupling term as is typically seen in the convective term in Navier–Stokes equation, while in the diffusively coupled map, the coupling term acts as a smoothing effect. Here we consider a model with nonlinear coupling, which has some similarity with a turbulent behavior in Navier–Stokes-type equation.

5.1. Soliton turbulence in a convective coupling model

Recalling the success of separation of procedure in the diffusively coupled map lattice model, we consider a model which consists of the following three procedures:

(1) Convective coupling (corresponding to the $-(v\nabla)v$ term in Navier–Stokes equation).

(2) Diffusion-type spatial average, which takes the same form as the diffusively coupled map lattice (corresponding to the $\nu\nabla^2v$ term in Navier–Stokes equation).

(3) Cut-off for high velocity: If we use only the above two procedures, (1) and (2), the system

exhibits a divergent behavior to infinity or, otherwise, is attracted to a trivial behavior like a fixed point. In order to remove this divergence and to take into account of the dissipation, we introduce a cut-off procedure. This is easily accomplished by $x'(i) = f(|x(i)|) * x(i)$ with monotonically decreasing function $f(x)$ with $f(0) = 1$ and $f(\infty) = 0$. Here we take $f(x) = \exp(-x^2/c)$.

Combining these three procedures, our coupled map lattice is given by

$$(I) \quad x'(i) = x_n(i) + (x_n(i-1) - x_n(i+1))x_n(i), \quad (10)$$

$$(II) \quad x''(i) = (1 - \epsilon)x'(i) + \epsilon/2(x'(i-1) + x'(i+1)), \quad (11)$$

$$(III) \quad x_{n+1}(i) = \exp(-x''(i)^2/c)x''(i). \quad (12)$$

The evolution $x_n(i) \rightarrow x_{n+1}(i, j)$ consists of the successive operation of the procedures (I), (II), and (III).

This model includes two parameters, c and ϵ , corresponding to the cut-off (related to the inverse

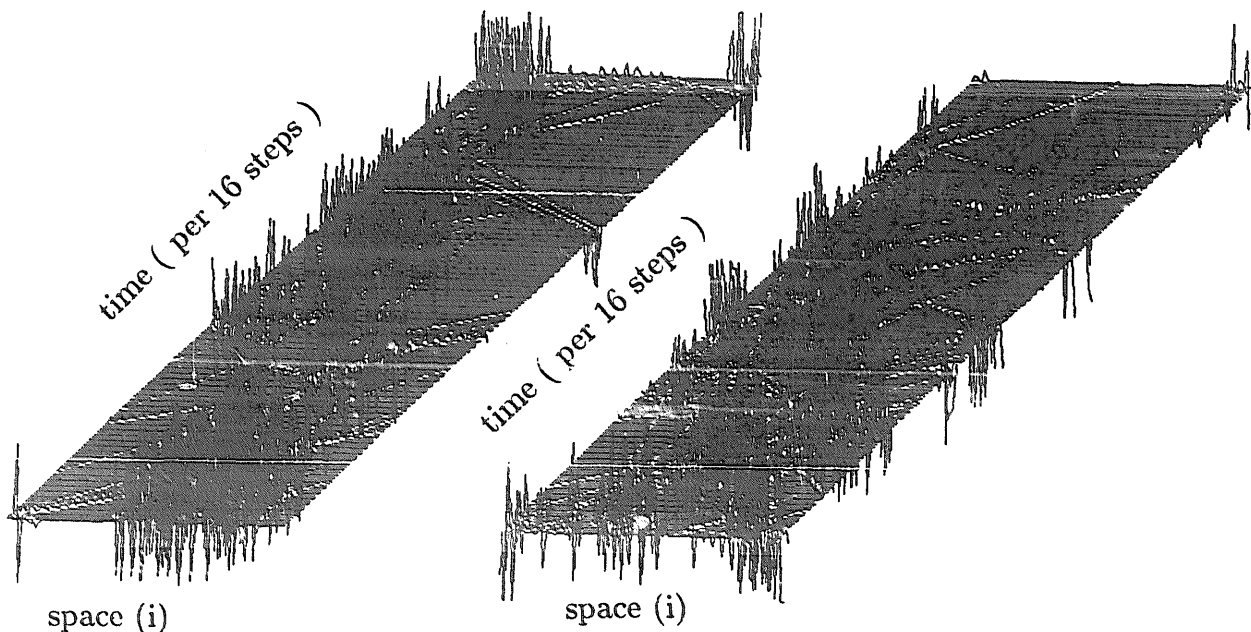


Fig. 13. Temporal evolution of pattern for the 1-dimensional convective coupling model with periodic boundary condition: $c = 300$, $\epsilon = 0.01$, $N = 100$, starting with a random initial condition. $x_n(i)$ for 1000–5000 (left), 5000–9000 (right) time steps is plotted per 16 steps.

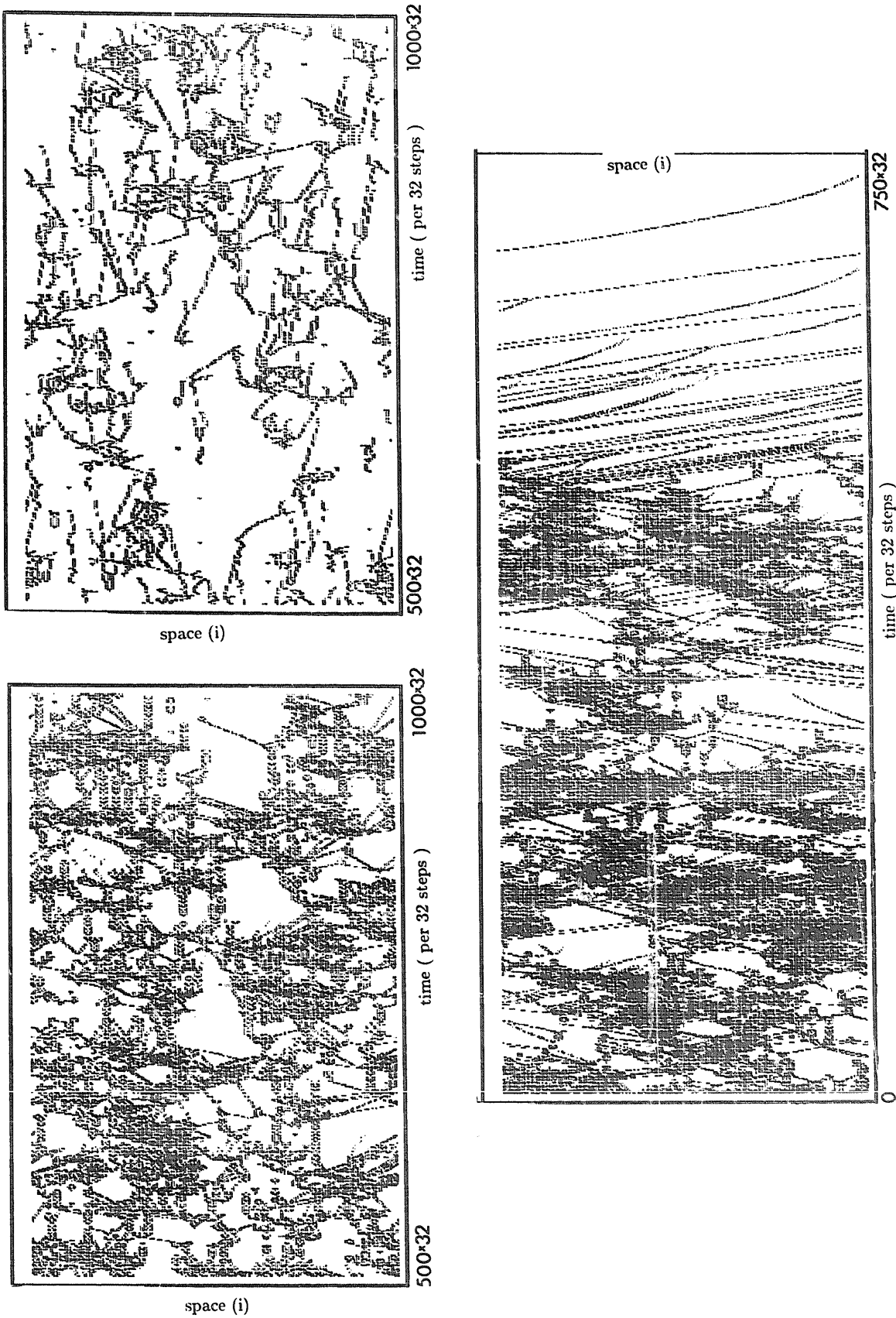


Fig. 14. Space-time derivative plot for the 1-dimensional convective coupling model, with periodic boundary condition, with $\epsilon = 0.01$, $N = 200$ and starting with a random initial condition. If $|x_n(t) - x_n(t+1)|$ is larger than 0.1, the corresponding space-time pixel is painted black, and for $0.03 < |x_n(t) - x_n(t+1)| < 0.1$ half of the pixel is painted, while it is left blank otherwise. (a) $\epsilon = 0.001$; $c = 2000$. For 16 000–32 000 time steps, plotted per 32 steps. (b) $\epsilon = 0.00001$; $c = 1 000 000$. For 16 000–32 000 time steps, plotted per 32 steps. (c) $\epsilon = 0.01$; $c = 350$. For 0–32 \times 750 time steps, plotted per 32 s.t.p.s. At the step about 32 \times 710, solitons disappear and the systems is attracted to a “dead” state.

of damping) and diffusion. As c is increased, the system starts to explore a region with larger non-linearity.

As c is increased, the following change occurs (for periodic boundary condition):

(1) The attractor is a “dead” state (i.e., $x(i) = 0$ for all i).

(2) The model exhibits a very long transient as “soliton turbulence” and finally is attracted to a dead state. If the size is larger this transient can be longer [28, 21, 22]. Also an addition of a small amount of noise makes this transient much longer.

(3) Soliton turbulence: We can see intermittent change among dead state, travelling of a localized wave (“soliton”) and chaotic bursts as an attractor. Soliton turbulence has first been found in a class of cellular automata [28, 29] and a coupled circle lattice [14, 4].

(4) Developed turbulent state: For larger c , no simple structure is observed.

The soliton turbulence here consists of the following processes (see fig. 13 for a temporal evolution of a pattern and fig. 14 for spatial derivative plots):

(1) Chaotic nucleus: By the nonlinear process (I), inhomogeneity in space is enhanced and then

hits the cut-off and decays. This process repeats chaotically (recall that the chaos is generated by a process of stretching and some saturation (folding)). Here we call it “nucleus”, since this localized structure is a nucleus which emits some solitons.

(2) Irregular emission of solitons from the chaotic nucleus.

(3) Travelling of solitons: In our model, the velocity of a soliton depends on its amplitude of solitons and its direction of the propagation is determined by the sign of $x(i)$ of a soliton. Since our model includes the cut-off for high velocity, the soliton loses its velocity and amplitude gradually.

(4) Collisions of solitons: By a collision two solitons form a chaotic nucleus or pass through or show the absorption, depending on their amplitudes and phases of collisions. If two colliding solitons have different directions, a pair-annihilation is also possible.

In our model we have seen the intermittent change between chaotic nucleus and a quiescent state ($x \approx 0$), in a wide parameter range. The time series at a given lattice point shows the intermittent change between a quiescent state and chaotic

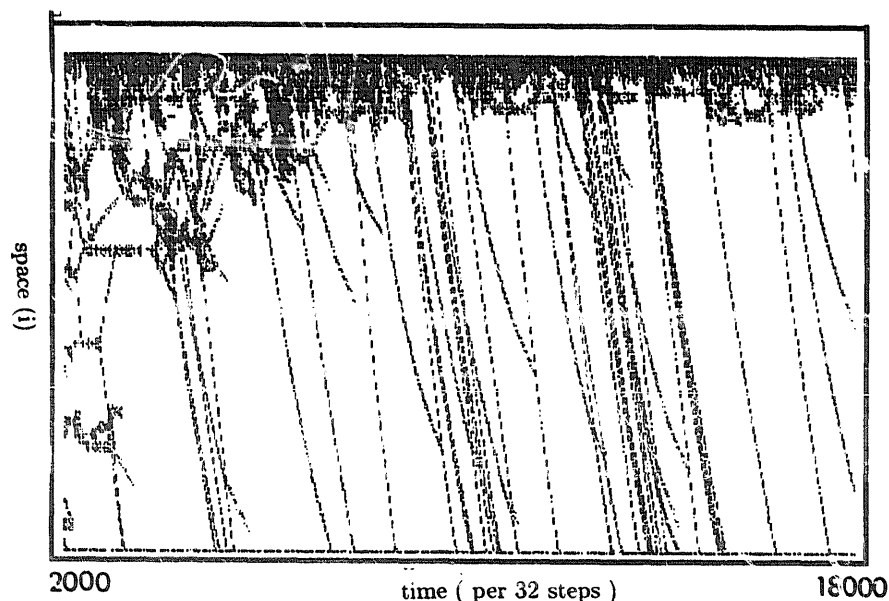


Fig. 15. Same figure as fig. 14 except the boundary condition: Here fixed boundary to $x(0) = 10.0$ at left end, and free at right end $x(N+1) = x(N)$. $\epsilon = 0.01$, $c = 250$. For 2000–18000 time steps plotted per 32 steps.

oscillation.

We note that the mechanism of the turbulence here consists of the formation of chaotic nucleus by the amplification of a small disturbance from a homogeneous state, its saturation by the damping and return to a homogeneous state. A similar mechanism for turbulence has recently been proposed as homoclinic excursions for a two-dimensional forced, damped, nonlinear Schrödinger equation [31].

If we use a fixed boundary condition at one end and a free boundary at the other end, we can construct a situation similar to an open flow experiment. In this case, some solitons are emitted to downflow from the chaotic region at the upper flow. The chaotic region changes its size with time, and behaves like a boundary layer in a fluid flow (see fig. 15).

5.2. 2-dimensional flow

The model (I)–(III) is straightforwardly extended to a flow in a two-dimensional system, by taking a two-dimensional vector $v(i, j) = (x(i, j), y(i, j))$ instead of the scalar quantity on a 2-dimensional lattice (i, j) . The procedure (I) is replaced by

$$(I') \quad x'(i, j) = x_n(i, j) + \left(\frac{1}{2}\right) [(x_n(i-1, j) - x_n(i+1, j))x_n(i, j) + (y_n(i, j-1) - x_n(i, j+1))x_n(i)], \quad (13)$$

$$(I') \quad y'(i, j) = y_n(i, j) + \left(\frac{1}{2}\right) [(x_n(i-1, j) - x_n(i+1, j))y_n(i, j) + (y_n(i, j-1) - x_n(i, j+1))y_n(i)], \quad (14)$$

while (II) is replaced by

$$(II') \quad x''(i, j) = \text{average of } x'(i, j) \\ = \text{for 13 neighbors } ((i \pm 1, j \pm 1), \\ (i \pm 2, j), (i, j \pm 2)),$$

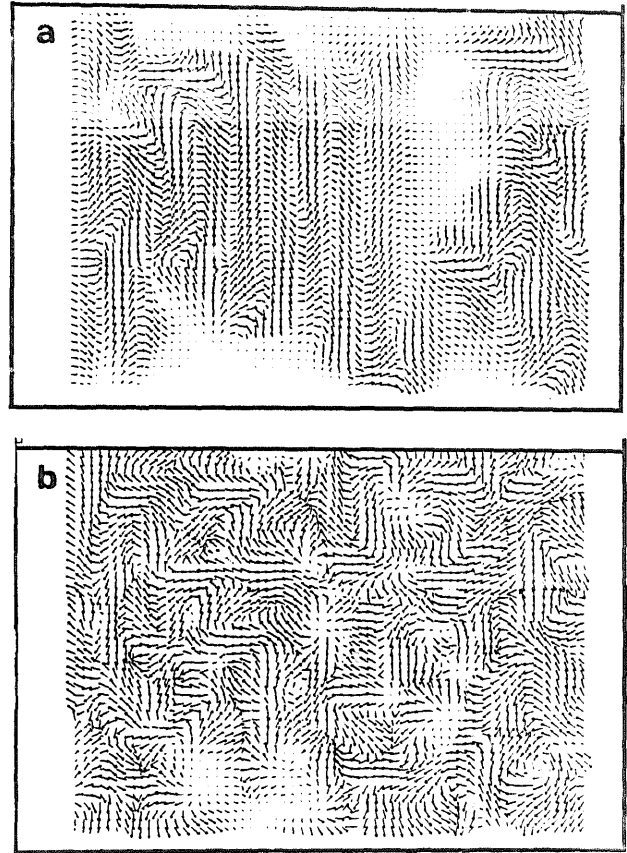


Fig. 16. Snapshot for the 2-dimensional convective coupling model (I')–(III'): Left boundary is fixed at $(v_L, 0)$ and right boundary is free. Top and bottom are rigid, i.e., $(x, y) = (0, 0)$. Lattice size is 63×48 . (a) $v_L = 3.0$, $c = 150$, time step = 60; (b) $v_L = 2.2$, $c = 300$, time step = 1281.

and (III) by

$$(III') \quad x_{n+1}(i, j) = x''(i, j) \exp \left(- \left(x''(i, j)^2 + y''(i, j)^2 \right) / c \right). \quad (15)$$

(Equation for $y(i, j)$ is just similar.)*

Examples of snapshots are shown in fig. 16, where the boundary condition is fixed at the left end and free at the right end, while it is fixed to zero at the top and bottom. We can see the

*The division by 2 in (I') is just a matter of convention, since the factor can be scaled out and be absorbed into the cutoff c .

formation of shocks, vortices, sinks, and sources (since we have not imposed the “incompressibility” condition in our model). The time series of a flow at a given lattice point shows the intermittent behavior, leading to the flicker-like temporal power spectra near the onset of chaotic motion.

5.3. Drawbacks

We have to admit that the model (I')–(III') is still a premature attempt towards the modelling of hydrodynamics, compared with the expanding field of lattice gas hydrodynamics [32]. Drawbacks in our model are the existence of artificial cut-off term (III) and a very rough treatment of the conservation law. In fact, our model has a conservation law only in the limit of small diffusion ($\epsilon \rightarrow 0$) and $c \rightarrow \infty$ (see fig. 14(b) for a case with very small ϵ and large c). One possible refinement of our model is to introduce another quantity corresponding to the density and to take into account a discrete version of the equation of continuity.

The strategy we have adopted here is to construct an artificial fluid dynamics model based on simple units corresponding to the convective term, diffusion, and damping. The existence of shocks, vortices, sinks, and sources in the present model suggests that the existence of these objects does not depend on the details of the equation, but just on the existence of the above units. We have not seen, however, a global parameter range in which the model exhibits the power-law for correlation function, as is seen in the inertial range in real fluid. This drawback is thought to come from the lack of conservation law. To proceed a realistic construction of fluid dynamics model, a detailed consideration on this point is required.

If the cut-off is not included, our model shows a trivial fixed point state (constant flow in the case of open flow boundary) or divergence to infinity, depending on the parameter. Near the critical point between these two phases, a state exhibits the soliton turbulence (for 1-d) or vortex turbulence (for 2-d) in a transient time regime, and then

decays to the fixed point or diverges to the infinity. Our cut-off procedure is a brute-force to suppress the divergence and preserve these “non-trivial stages as attractors. In a real fluid, this critical state is thought to be preserved not by this artificial method but via the conservation law [33].

6. Summary and future problems

Pattern dynamics in a one-dimensional diffusively coupled map lattice is reported, with the emphasis on the transition between a frozen random pattern and a pattern selection. In a 2-dimensional lattice, the pattern dynamics has turned out to be quite similar to the 1-dimensional case if the coupling is small, while no frozen pattern is seen in the strong coupling regime. This is thought to be due to the dominancy of the diffusion effect at the domain boundary, which is simply estimated as $M^{(1-1/d)}$ for a dimension d and a domain of size M . Thus it is expected that a frozen pattern is much harder to appear in a 3-dimensional lattice. Of course, more elaborated argument analogous to the Peierls' in an equilibrium phase transition should be made in future.

Our results in 1-d and 2-d lattices show a remarkable similarity with recent experiments on Bénard convection [20], electrical convection in liquid crystal, [25], and Faraday instability in water wave [26]. (see also [34–36] for experiments on the spatiotemporal chaos which may have some connections with our simulation here). The similarity may not be surprising if we think that our model is just a prototype of a system with chaotic mechanism and spatial diffusion. In future, quantitative comparison with our model and their experiments should be made.

In section 5, we have considered some models with convective coupling. The coexistence of solitons or vortices and turbulent burst is noted in the transition parameter range, where the intermittent change among these patterns is observed. This gives us a hope, that, if suitably refined, some coupled map lattice for hydrodynamics may be

constructed. This construction is of interest not only from a dynamical system theoretical but also from a practical viewpoint (note that all the simulations here are carried out by SUN-computer, not by CRAY).

Use of coupled map lattice for physical phenomena have just been started. One of the best success in this application has been carried out by Oono and Puri for the problem of spinodal decomposition [37]. Indeed, their model gives a much faster simulator than the conventional Monte Carlo method. A similar modelling is possible in the roll formation in convection, crystal growth, complex Ginzburg–Landau equation, and so on. Also the use of coupled circle lattice for the Josephson array and charge density wave will be promising. For the application, our guiding principle is to decompose the dynamics into some parts and separate the procedure to local parts and spatial coupling parts.

Up to now there is no relevant theory on spatiotemporal chaos. The argument on the preimages in section 1 makes the use of Perron–Frobenius operator possible [38]. With the use of the standard argument of the decomposition into subsystem and heat bath, we can construct a mean-field-type approximation on the invariant measure [39]. It is also important to search for a statistical mechanical theory based on this operator as has been successful in a low-dimensional chaos [40, 41].

Through this statistical mechanical study, we hope to understand the transition among pattern dynamics in spatiotemporal chaos.

Acknowledgements

The author would like to thank J.P. Crutchfield, M. Sano, K. Ikeda, Y. Oono, T. Ikegami, N.H. Packard, G. Mayer-Kress, D.K. Umbarger and J.D. Farmer for useful discussions. He would also like to thank P.C. Hohenberg and H. Sompolinsky for illuminating questions on the previous paper [1]. He is also grateful to S. Ciliberto, N. Tuffillaro,

and S. Nasuno and M. Sano for the information and discussion of their experiments prior to their publications. The author is thankful to the Ministry of Education, Japan for financial support for the stay at Illinois and to the people in CCSR and CNLS for their hospitality during his stay.

References

- [1] K. Kaneko, Pattern dynamics in spatiotemporal chaos, *Physica D* 34 (1989) 1.
- [2] K. Kaneko, *Progr. Theor. Phys.* 72 (1984) 480; 74 (1985) 1033.
- [3] K. Kaneko, Ph.D. thesis, Collapse of tori and genesis of chaos in dissipative systems, 1983 (enlarged version is published by World Scientific, Singapore, 1986).
- [4] J.P. Crutchfield and K. Kaneko, Phenomenology of spatiotemporal chaos, in: *Directions in Chaos* (World Scientific, Singapore, 1987).
- [5] I. Waller and R. Kapral, *Phys. Rev. A* 30 (1984) 2047. R. Kapral, *Phys. Rev. A* 31 (1985) 3868.
- [6] K. Kaneko, *Physica D* 23 (1986) 436.
- [7] T. Yamada and H. Fujisaka, *Progr. Theor. Phys.* 72 (1985) 885.
- [8] J.D. Keeler and J.D. Farmer, *Physica D* 23 (1986) 413.
- [9] R.J. Deissler, *Phys. Lett. A* 120 (1987) 334.
K. Kaneko, *Phys. Lett. A* 111 (1985) 321.
R.J. Deissler and K. Kaneko, *Phys. Lett. A* 119 (1987) 397.
F. Kaspar and H.G. Schuster, *Phys. Lett. A* 113 (1986) 451.
F. Kaspar and H.G. Schuster, *Phys. Rev. A* 36 (1987) 842.
P. Alstrom and R.K. Ritala, *Phys. Rev. A* 35 (1987) 300.
S. Coppersmith, *Phys. Rev. A* 38 (1988) 375.
K. Aoki and N. Mugibayashi, *Phys. Lett. A* 128 (1988) 349.
P. Grassberger, Lumped and distributed dynamical systems, preprint (1987).
G. Mayer-Kress and K. Kaneko, to appear in *J. Stat. Phys.*
- [10] For CML see also: K. Kaneko and T. Konishi, *J. Phys. Soc. Jpn.* 56 (1987) 2993 and preprint (Los Alamos, 1988).
I. Tsuda and H. Shimizu, in: *Complex Systems—Operational Approaches*, H. Haken, ed. (Springer, Berlin, 1985).
M. Rotenberg, *Physica D* 30 (1988) 192.
J. Brindley and R.M. Everson, *Phys. Lett. A* 134 (1989) 229.
L.A. Bunimovich and Ya.G. Sinai, *Nonlinearity* 1 (1988) 491.
I.S. Aronson, A.V. Gaponov–Grekhov, and M.I. Rabinovich, *Physica D* 33 (1988) 1.
D. Rand and T. Bohr, preprint (1988).
M.H. Jensen, preprint (1988).
L.A. Bunimovich, A. Lambert and R. Lima, preprint (1989).

- [11] K. Kaneko, *Phys. Lett. A* 125 (1987) 25; *Eur. Phys. Lett.* 6 (1988) 193.
- [12] For CML with global coupling (mean-field-type model for (1)): see K. Kaneko, *Chaotic but Regular Posi-Nega Switch Among Coded Attractors by Cluster Size Variation*, preprint (Los Alamos, 1989); *Clustering, Switching, Coding, and Hierarchical Ordering in Globally Coupled Chaotic Systems*, preprint (Los Alamos, 1989). See also P. Hadley and K. Wiesenfeld, preprint (1989).
- [13] See e.g., A.J. Lichtenberg and M.A. Lieberman, *Regular and Stochastic Motion* (Springer, Berlin, 1983). K. Kaneko and R.J. Bagley, *Phys. Lett. A* 110 (1985) 435. K. Kaneko, *Phys. Lett. A* 129 (1988) 9.
- [14] K. Kaneko, *Phenomenology and characterization of spatio-temporal chaos*, in: *Dynamical Systems and Singular Phenomena*, G. Ikegami, ed (World Scientific, Singapore, 1987).
- [15] See for a possible reduction to probabilistic cellular automata (CA), K. Kaneko, in: *Dynamical Problems in Soliton Systems*, S. Takeno, ed. (Springer, Berlin, 1985), pp. 272–277.
- [16] H. Chate and P. Manneville, *C.R. Acad. Sci.* 304 (1987) 609; *Phys. Rev. Lett.* 58 (1987) 112.
- [17] H. Chate and P. Manneville, *Physica D* (to appear); *Phys. Rev. A* (to appear).
- [18] This is essentially the extension of the notion of Brownian motion of chaotic defect in a 1-dimensional lattice [11, 1].
- [19] See for the argument on a possible relation of spatiotemporal intermittency with directed percolation (S.P. Obukhov, *Physica A* 101 (1980) 145), Y. Pomeau, *Physica D* 23 (1986) 3. According to [17], however, the universality class on critical exponents seems to be different.
- [20] S. Ciliberto and P. Bigazzi, *Phys. Rev. Lett.* 60 (1988) 286 and private communications.
- [21] J.P. Crutchfield and K. Kaneko, *Phys. Rev. Lett.* 60 (1988) 2715.
- [22] J.P. Crutchfield and K. Kaneko, in preparation.
- [23] K. Kaneko and D.K. Umberger, to be published.
- [24] For another example of a 2-dimensional logistic lattice (with a linear coupling), see G.L. Oppo and R. Kapral, *Phys. Rev. A* 33 (1986) 4219.
- [25] S. Nasuno, M. Sano and Y. Sawada, private communications. To be published.
- [26] See also, N. Tuffiaro and J. Gollub, private communication.
- [27] See also, T. Bohr and S. Rasmussen, *Phys. Lett. A* 125 (1987) 107.
- [28] K. Kaneko, in: *Theory and Applications of Cellular Automata*, S. Wolfram, ed. (World Scientific, Singapore, 1986), pp. 367–399.
- [29] Y. Aizawa, I. Nishikawa and K. Kaneko, in preparation.
- [30] K. Kaneko and Y. Akutsu, *Phase transition in two-dimensional stochastic cellular automata*, *J. Phys. A* 19 (1986) L69–74.
- [31] A.C. Newell, D. Rand and D. Russel, to appear in *Phys. Lett. A*.
- [32] U. Frisch, B. Hasslacher and Y. Pomeau, *Phys. Rev. Lett.* 56 (1986) 1505. S. Wolfram, *J. Stat. Phys.* 45 (1986) 471. Special issue of *Complex Systems* 1 (1987) No. 4.
- [33] This picture, in some sense, reminds us of the recent “self-organized critical state”: P. Bak, C. Tang and K. Wiesenfeld, *Phys. Rev. Lett.* 59 (1987) 381.
- [34] S. Sato, M. Sano and Y. Sawada, *Phys. Rev. A* 37 (1988) 1679.
- [35] R.J. Donnelly et al., *Phys. Rev. Lett.* 44 (1980) 987.
- [36] M. Lowe, J.P. Gollub and T.C. Lubensky, *Phys. Rev. Lett.* 51 (1983) 786.
- [37] Y. Oono and S. Puri, *Phys. Rev. Lett.* 58 (1986) 836 and preprints, to appear in *Phys. Rev. A*.
- [38] K. Kaneko, preprint (Los Alamos, 1989).
- [39] See for the application of this method to CA, H.A. Gutowitz, J.D. Victor, and B.W. Knight, *Physica D* 29 (1987) 18.
- [40] R. Bowen and D. Ruelle, *Inventiones Math.* 29 (1975) 181. D. Ruelle, *Thermodynamic Formalism* (Addison Wesley, Reading, MA, 1978).
- [41] Y. Oono and Y. Takahashi, *Progr. Theor. Phys.* 63 (1980) 1804.